Curvature profiles as initial conditions for primordial black hole formation

2007 Class. Quantum Grav. 24 1405

(http://iopscience.iop.org/0264-9381/24/6/003)

IOP Publishing Classical and Quantum Gravity

Class. Quantum Grav. **24** (2007) 1405–1431 doi:10.1088/0264-9381/24/6/003

Curvature profiles as initial conditions for primordial black hole formation

Alexander G Polnarev and Ilia Musco

Astronomy Unit, Queen Mary University of London, Mile End Road, London E1 4NS, UK

Received 16 July 2006, in final form 8 February 2007
Published 6 March 2007
Online at stacks.iop.org/CQG/24/1405

Abstract

This work is part of an ongoing research programme to study possible primordial black hole (PBH) formation during the radiation-dominated era of the early universe. Working within spherical symmetry, we specify an initial configuration in terms of a curvature profile, which represents initial conditions for the large amplitude metric perturbations, away from the homogeneous Friedmann–Robertson–Walker model, which are required for PBH formation. Using an asymptotic quasi-homogeneous solution, we relate the curvature profile with the density and velocity fields, which at an early enough time, when the length scale of the configuration is much larger than the cosmological horizon, can be treated as small perturbations of the background values. We present general analytic solutions for the density and velocity profiles. These solutions enable us to consider in a self-consistent way the formation of PBHs in a wide variety of cosmological situations with the cosmological fluid being treated as an arbitrary mixture of different components with different equations of state. We obtain the analytical solutions for the density and velocity profiles as functions of the initial time. We then use two different parametrizations for the curvature profile and follow numerically the evolution of initial configurations.

PACS number: 09.70.−s

1. Introduction

The possible existence of primordial black holes (PBHs) was first proposed in 1966 by Zeldovich and Novikov [1] and, at the beginning of 1970s, by Hawking [2]. It was then widely discussed in the following years (see, for example the recent review by Carr for a full list of references [3]). In 1974 Hawking made his famous discovery of black hole evaporation [4], that is cosmologically relevant if the mass of the black holes concerned is less than 10^{15} g.

For this reason the problem of PBH formation started to be attractive and it was widely investigated in the following 30 years.

The PBH formation process was first investigated by Carr (1975) [5] using a simplified model for an overdense collapsing region, described as a closed Friedmann–Robertson–Walker (FRW) universe, surrounded by a spatially flat FRW expanding background. In the radiation-dominated epoch of the universe this leads to a threshold value for the perturbation amplitude δ_c, where the amplitude δ is defined as the mass excess in the overdense region, and the black holes formed have masses of the order of the horizon mass at the time of formation. In this way Carr obtained a first rough estimate of $\delta_c \sim 1/3$ (evaluated at the time of horizon crossing, when the overdensity region enters into the cosmological horizon) by comparing the Jeans length with the cosmological horizon scale at the time of black hole formation. Subsequently a self-consistent hydrodynamical analysis of PBH formation was carried out by Nadezhin, Novikov and Polnarev in 1978 [6] and in 1980 [7] using, for the first time in this context, a hydrodynamical computer code written in the Misner–Sharp slicing, characterized by a diagonal metric with a cosmic time coordinate that reduces to the FRW metric in the absence of perturbations. Previously the same slicing was used by Podurets [8] and May and White [9] to study stellar core collapse. An alternative analysis was developed in 1979 by Bicknell and Henriksen [10] using a different method based on integration along hydrodynamical characteristics. These papers showed that the threshold amplitude of the perturbation is dependent on the particular shape of the initial conditions. It was also found in [6] that pressure gradients considerably reduce the PBH mass formed at the end of the hydrodynamical process.

In the following 20 years attention was concentrated on different aspects of PBH formation. For example, calculating the amount of Hawking radiation emitted by sufficiently small PBHs, with a mass less than 10^{15} g, one can obtain important constraints on parameters that characterize the different epochs and processes of the universe (see, for example, [11, 12] and references given there). The formation of PBHs was considered also within different scenarios, for example during phase transitions [13], with a soft equation of state [14], by collapse of cosmic loops [15, 16] or from bubble collisions [17]. In general, the study of PBHs provides a unique probe for different areas of physics: the early universe, quantum gravity, gravitational collapse and high energy physics. This is explained with full lists of references in the various reviews of PBHs (see, for example [3]).

More recently, in 1999, Niemeyer and Jedamzik [18, 19] made new numerical calculations pointing out the relevance of scaling laws for PBH formation. They showed that the black hole mass $M_{\rm BH}$ follows a power law $(\delta - \delta_c)^\gamma$ if δ is close enough to δ_c, the same behaviour as seen in critical collapse by Choptuik [20] and other authors (see review [21]). Niemeyer and Jedamzik found that $\delta_c \simeq 0.7$ for the three types of perturbation profile that they studied. In the same year, Shibata and Sasaki [22] presented an alternative formalism for studying PBH formation focusing on metric perturbations, rather than density perturbations, as had also been done previously [6, 23]. They pointed out that the initial conditions used in [19] were specified initially within a nonlinear regime of perturbations of the energy density and velocity field, and were therefore 'inevitably contaminated by an unrealistic decaying mode' component that would diverge for $t \to 0$. In a recent paper [24] this analysis has been converted in terms of the perturbation amplitude δ, showing that the Shibata and Sasaki results, corresponding to a wide choice of perturbation shapes, are consistent with δ_c in the range $0.3 \lesssim \delta_c \lesssim 0.5$.

The disagreement between this and the value $\delta_c \simeq 0.7$ has been explained by Musco *et al* [25], where simulations similar to those used in [18] were carried out but specifying the initial conditions within the linear regime of energy density perturbations, giving only growing

solutions at the horizon crossing time. The simulations in [25] give values of δ_c in the range 0.43–0.47 (instead of 0.67–0.71) for the same types of perturbation profiles used in [19].

The present work is a new analysis of PBH formation using the numerical technique developed in [25], implemented together with a quasi-homogeneous solution that, assuming spherical symmetry, can be characterized by a single function of the radial coordinate. In this paper this function, denoted by $K(r)$, is chosen as a curvature profile that allows a self-consistent determination to be made of the whole set of initial conditions. This is a further development of the original approach of Nadezhin, Novikov and Polnarev [6].

According to the asymptotic quasi-homogeneous solution [30] (valid as $t \to 0$), an arbitrary curvature profile $K(r)$ corresponding to a large amplitude perturbation of the metric does not depend on time, while perturbations of energy density and velocity vanish asymptotically as $t \to 0$. Therefore these can be treated as small perturbations. Solving the equations for the small velocity and density perturbations analytically we impose in a self-consistent way all of the initial conditions corresponding to a moment in time when the quasi-homogeneous solution of a certain order is valid. The curvature profile $K(r)$ appears as the source in the right-hand side of the relevant equations and we can say that the density and velocity perturbations which we use as initial conditions are generated by the curvature $K(r)$. Then we use the computer code to follow the subsequent nonlinear evolution of the initial configuration (by the configuration we mean the region of strong metric perturbation). To avoid confusion we should emphasize that the small perturbations predicted by any cosmological model are relevant in this context only when one calculates the probability of finding a configuration with a high amplitude perturbation of the metric. In fact, the small perturbations of density and velocity which we discuss here are not linear cosmological initial conditions, but entirely determined from the curvature profile within the initial configuration.

The paper is organized as follows.

In section 2 we give a very brief description of the Misner–Sharp equations. We then use these equations to specify all of the initial conditions, which we then use in our numerical computations, in terms of a curvature profile. When the length scale of the configuration is much larger than the cosmological horizon, the Misner–Sharp equations can be reduced to a system of linear differential equations which we solve analytically.

In section 3 we obtain solutions for a rather general case corresponding to an arbitrary mixture of perfect fluids. We demonstrate that, in the simple case of a single perfect fluid, corresponding perturbations of energy density and velocity, obtained within the framework of the quasi-homogeneous solution, evolve with time like a pure growing mode in standard cosmological perturbation theory, while their space dependence is entirely determined by the curvature profile $K(r)$.

In section 4 we discuss the physical properties of the curvature profile $K(r)$. In section 5 we introduce two different parametrizations of $K(r)$. In section 6, we present numerical tests to demonstrate self-consistency of the initial conditions. We then show that the initial conditions described by the quasi-homogeneous solution have been imposed consistently in the code and give numerical examples of primordial black hole formation in the case of a radiation-dominated universe. We show how the threshold for black hole formation is linked with the curvature profile and discuss the results obtained with the two different parametrizations used in the computations.

Summary and conclusions are given in section 7.

2. Mathematical formulation of the problem

2.1. The Misner–Sharp equations

Assuming spherical symmetry, it is convenient to divide the collapsing matter into a system of concentric spherical shells and to label each shell with a Lagrangian comoving radial coordinate which we denote as r. Then the metric can be written in the form used by Misner and Sharp [26]:

$$ds^2 = -a^2 dt^2 + b^2 dr^2 + R^2(d\theta^2 + \sin^2\theta\, d\varphi^2), \tag{1}$$

where R is a circumference coordinate, a and b are functions of r and of the time coordinate t, which reduces to the familiar FRW time coordinate (referred to in literature as 'cosmic time') in the absence of perturbations. The FRW metric used to describe homogeneous and isotropic cosmological models is a particular case of (1):

$$ds^2 = -dt^2 + s^2(t)\left[\frac{dr^2}{1 - Kr^2} + r^2(d\theta^2 + \sin^2\theta\, d\phi^2)\right], \tag{2}$$

where $s(t)$ is the scale factor and K is the curvature parameter that is equal to $0, +1$ and -1 for flat, closed and open universes.

For a classical fluid, composed of particles with nonzero rest mass, it is convenient to use the rest mass μ contained interior to the surface of a shell (or, equivalently, the baryon number) as its comoving coordinate r. For a classical fluid, composed of particles with nonzero rest mass, it is convenient to use the rest mass μ contained interior to the surface of a shell (or, equivalently, the baryon number) as its comoving coordinate r. For fluids not possessing these conserved quantities, one can still define a 'relative compression factor' ρ [27, 28] which then plays the same role as that played by the rest-mass density for standard fluids but which has dimensions of $1/\text{volume}$. The relationship between μ and r is then given by

$$d\mu = 4\pi\rho R^2 b\, dr. \tag{3}$$

Identifying μ and r one gets

$$b = \frac{1}{4\pi R^2 \rho}. \tag{4}$$

Note that in this formulation, b has dimensions of length while r and μ are dimensionless. Following the notation of [26], we write the equations in terms of the operators. Following the notation of [26], we write the equations in terms of the operators

$$D_t \equiv \frac{1}{a}\left(\frac{\partial}{\partial t}\right), \tag{5}$$

$$D_r \equiv \frac{1}{b}\left(\frac{\partial}{\partial \mu}\right), \tag{6}$$

and define

$$U \equiv D_t R, \tag{7}$$

$$\Gamma \equiv D_r R, \tag{8}$$

where U is the radial component of the 4-velocity in the associated Eulerian frame, R is the circumference coordinate, and Γ is a generalization of the Lorentz factor.

The system of Einstein equations can be written as

$$D_t U = -\left[\frac{\Gamma}{(e+p)} D_r p + \frac{M}{R^2} + 4\pi R p\right], \tag{9}$$

$$D_t \rho = -\frac{\rho}{\Gamma R^2} D_r (R^2 U), \tag{10}$$

$$D_t e = \frac{e+p}{\rho} D_t \rho, \tag{11}$$

$$D_t M = 4\pi p U R^2, \tag{12}$$

$$D_r a = -\frac{a}{e+p} D_r p, \tag{13}$$

$$D_r M = 4\pi \Gamma e R^2, \tag{14}$$

where M is the mass energy contained inside radius μ, e is the energy density, p is the pressure and Γ can be calculated either from (8) or from the constraint equation

$$\Gamma^2 = 1 + U^2 - \frac{2M}{R}. \tag{15}$$

To solve this system of equations one needs to specify also an equation of state. For doing this we take the matter to be a mixture of n ideal fluids with ith component having energy density e_i and pressure p_i. Hence we should work with the following equation of state

$$p = p(e_1, e_2, \ldots e_n) v = \sum_{i=1}^{n} \gamma_i e_i, \tag{16}$$

where all of the γ_i are constants, but to simplify our calculations we will replace this equation of state by the phenomenological relationship

$$p = \gamma(t) e, \tag{17}$$

that we will call an 'effective equation of state' (the function $\gamma(t)$ is defined in section 3).

When the cosmic time approach is used for calculations of gravitational collapse leading to black hole formation it has the well-known drawback that singularities unavoidably appear after a finite time in numerical calculations and subsequent evolution cannot then be followed. This has the consequence that the later stages of the evolution which could potentially be seen by an outside observer cannot be numerically followed in this slicing and, in particular, it is not possible to follow all of the process of the formation of the black hole. This drawback is the reason for an observer-time formulation being used in the present work rather than continuing to use the cosmic time formulation. Hernandez and Misner [29] introduced the concept of 'observer time', using as the time coordinate the time at which an outgoing radial light ray emanating from an event reaches a distant observer. In the original formulation, this observer was placed at future null infinity but for calculations in an expanding cosmological background we use an FRW fundamental observer sufficiently far from the perturbed region so as to be unaffected by the perturbation. A complete description of the Hernandez–Misner equations was given in [25].

2.2. Perturbations in the quasi-homogeneous solution

To provide initial data for our calculation of PBH formation, we follow the quasi-homogeneous approach ([6, 7]) and solve the Misner–Sharp system of equations, giving a non-perturbative

description of large amplitude metric perturbations away from the homogeneous FRW model. Using this approach, as mentioned in the introduction, we can avoid the unphysical arbitrariness in the choice of initial conditions.

The characteristic feature of the asymptotic quasi-homogeneous solution is that, when $t \to 0$, all mass elements expand asymptotically, according to the FRW model, with energy density $e = 1/6(1+\gamma)^2\pi t^2$ for an equation of state given by (16), while a spatial hypersurface with $t = \text{const}$ can have arbitrary curvature if the perturbation has a length scale sufficiently larger than the cosmological horizon. As a consequence of this the hydrodynamical quantities can be considered as small perturbations with respect to the background solution, while the curvature perturbation is arbitrarily large. This curvature perturbation is time independent in this regime, because pressure gradients are then negligible [6, 30].

In this work, we consider spherical symmetry and specify conditions on an initial spacelike hypersurface using a time-independent function $K = K(r)$ that represents the curvature profile. We can also see that introducing a profile $K(r)$ into the Friedmann–Robertson–Walker metric (2) one obtains an asymptotic solution of the Einstein equation in the limit $t \to 0$. We therefore use $K(r)$ to represent initial curvature perturbations with scales much larger than the horizon, and solve the system of perturbed differential equations to express the set of hydrodynamical variables in terms of $K(r)$.

The system of equations (7)–(15) can be rewritten as

$$\dot{R} = aU \tag{18}$$

$$\frac{\dot{b}}{b} = a\frac{U'}{R'} \tag{19}$$

$$\frac{a'}{a} = -\frac{\gamma}{1+\gamma}\frac{e'}{e} \tag{20}$$

$$\dot{M} = -4\pi\gamma e R^2 \dot{R} \tag{21}$$

$$M' = 4\pi e R^2 R' \tag{22}$$

$$\frac{R'^2}{b^2} = 1 + U^2 - \frac{2M}{R}, \tag{23}$$

where the dot and dash denote differentiation with respect to t and r, respectively; we use the effective equation of state (17) to express the pressure as a function of the energy density, equation (8) gives an expression for Γ, and ρ can be calculated from equation (10).

The background solution is a spatially flat FRW universe described by $K = 0$. The corresponding value of the energy density (indicated with the suffix 'b') is calculated from the Friedmann equation

$$\left(\frac{\dot{s}}{s}\right)^2 = H_{\rm b}^2 = \frac{8\pi}{3}e_{\rm b}. \tag{24}$$

The quantity e_b is related to the scale factor $s(t)$ by equation (21) used for the unperturbed case

$$\frac{\dot{e}_b}{e_b} = -3(1+\gamma)\frac{\dot{s}}{s}, \tag{25}$$

while the background values of the other quantities are obtained from the FRW metric (2) and the set of equations (18)–(23):

$$a_{\rm b} = 1 \tag{26}$$

$$b_{\rm b} = s(t) \tag{27}$$

$$R_{\rm b} = s(t)r \tag{28}$$

$$M_{\rm b} = \frac{4}{3}\pi e_{\rm b} R_{\rm b}^3 \tag{29}$$

$$U_{\rm b} = H_{\rm b} R_{\rm b} = \dot{s}(t)r. \tag{30}$$

As already mentioned, when the perturbation is well outside the cosmological horizon, all of the hydrodynamical quantities have nearly homogeneous profiles with their perturbations being small deviations away from the uniform solution. It is useful therefore to parametrize the scale of the perturbations using a dimensionless parameter ϵ that gives explicitly the ratio of the cosmological horizon scale $R_H = H_{\rm b}^{-1}$ to the physical length scale of the configuration

$$R_0 = s(t)r_0, \tag{31}$$

where r_0 is the comoving radius of the configuration. Therefore we have

$$\epsilon \equiv \left(\frac{R_H}{R_0}\right)^2 = \left(\frac{1}{H_{\rm b} s r_0}\right)^2 = \frac{1}{\dot{s}^2 r_0^2} \equiv \frac{1}{N^2} \ll 1, \tag{32}$$

where N is the number of horizon scales inside the configuration ($R_0 = N R_H$). From this equation it is clear that ϵ is a function only of time, and its time derivative, as follows from (25), is given by

$$\frac{\dot{\epsilon}}{\epsilon} = -2\frac{\dot{s}}{s} - \frac{\dot{e}_{\rm b}}{e_{\rm b}} = -2\frac{\dot{s}}{s} + 3(1+\gamma)\frac{\dot{s}}{s} = (1+3\gamma)\frac{\dot{s}}{s}. \tag{33}$$

We treat ϵ as a small parameter for our asymptotic solution, and this will allow us to keep only terms of first order in ϵ in the hydrodynamical equations (18)–(23) when we use these equations to obtain the asymptotic quasi-homogeneous solution. From equations (31) and (33) one can relate the scale factor to r_0

$$s(t) = \frac{N R_H}{r_0}, \tag{34}$$

and we can use this to define the comoving coordinate as

$$r = \frac{R_{\rm b}}{s(t)} = \frac{r_0}{N R_H} R_{\rm b}, \tag{35}$$

where the value of $R_{\rm b}$ is obtained by integrating equation (3),

$$R_{\rm b} = \left(\frac{\mu}{4\pi\rho}\right)^{1/3} \tag{36}$$

while r_0 will be obtained from the curvature profile (see sections 4 and 5).

The initial perturbations are defined as

$$R = R_b(1 + \epsilon\tilde{R}) \tag{37}$$

$$U = H_b R(1 + \epsilon\tilde{U}) \tag{38}$$

$$b = \frac{R'}{\sqrt{1 - K(r)r^2}}(1 + \epsilon\tilde{b}) \tag{39}$$

$$a = 1 + \epsilon\tilde{a} \tag{40}$$

$$e = e_b(1 + \epsilon\tilde{e}) \tag{41}$$

$$M = \frac{4}{3}\pi e_b R^3 (1 + \epsilon \tilde{M}). \tag{42}$$

The tilde quantities are in general functions of both r and t. It is convenient to define a new independent time variable $\xi \equiv \ln(s)$ given by

$$\frac{\dot{s}}{s}\frac{\partial}{\partial t} = \frac{\partial}{\partial \xi}. \tag{43}$$

Starting from equation (18), and using expressions (35), (38) and (40) we get

$$\frac{\dot{s}}{s} + (\epsilon \tilde{R})^{\cdot} = \frac{\dot{s}}{s}(1 + \epsilon \tilde{a})(1 + \epsilon \tilde{U}),$$

then linearizing this equation and using (33) and (43) one obtains

$$(1 + 3\gamma)\tilde{R} + \frac{\partial \tilde{R}}{\partial \xi} = \tilde{a} + \tilde{U}. \tag{44}$$

Similarly, perturbing equation (19) we get

$$(\epsilon \tilde{b})^{\cdot} = -\epsilon \frac{\tilde{a}' U}{R'}$$

and then, using (33), we have

$$(1 + 3\gamma)\tilde{b} + \frac{\partial \tilde{b}}{\partial \xi} = -r\tilde{a}'. \tag{45}$$

Perturbing equation (20) and integrating it over r we have

$$(1 + \gamma)\tilde{a} + \gamma \tilde{e} = 0. \tag{46}$$

Perturbing equation (21) to first order in ϵ we get

$$\frac{1}{3}(1 + \epsilon \tilde{M})\left[\frac{\dot{e}_b}{e_b} + 3\frac{\dot{R}}{R} + (\epsilon \tilde{M})^{\cdot}\right] = -\gamma(1 + \epsilon \tilde{e})\frac{\dot{R}}{R}, \tag{47}$$

and, using (25), (42) can be rewritten as

$$-3(1 + \gamma)\frac{\dot{s}}{s} + 3(1 + \gamma)\frac{\dot{R}}{R} - 3(1 + \gamma)\frac{\dot{s}}{s}\epsilon \tilde{M} + (\epsilon \tilde{M})^{\cdot} + 3\frac{\dot{R}}{R}\epsilon \tilde{M} + 3\gamma \frac{\dot{R}}{R}\epsilon \tilde{e} = 0.$$

Using equation (36) we get

$$\dot{\epsilon}\tilde{M} + \epsilon \dot{\tilde{M}} - 3\gamma \frac{\dot{s}}{s}\epsilon \tilde{M} + 3\gamma \frac{\dot{s}}{s}\epsilon \tilde{e} + 3(1 + \gamma)(\dot{\epsilon}\tilde{R} + \epsilon \dot{\tilde{R}}) = 0,$$

and finally using equations (33), (43), (44) and (46) we have

$$\tilde{M} + \frac{\partial \tilde{M}}{\partial \xi} = -3(1 + \gamma)\tilde{U}. \tag{48}$$

Perturbing equation (22) we obtain

$$(1 + \epsilon \tilde{M})\frac{R'}{R} + \frac{1}{3}\epsilon \tilde{M}' = (1 + \epsilon \tilde{e})\frac{R'}{R},$$

that can be rewritten as

$$\tilde{e} = \frac{1}{3r^2}(r^3 \tilde{M})'. \tag{49}$$

Perturbing equation (23), we have

$$[(1 - K(r)r^2)(1 - 2\epsilon \tilde{b}) - 1] = \frac{\dot{s}^2}{s^2}R^2(1 + 2\epsilon \tilde{U}) - \frac{8\pi e_b R^2}{3}(1 + \epsilon \tilde{M}),$$

that using (24) becomes

$$-[K(r)r^2 + 2\epsilon\tilde{b}(1 - K(r)r^2)] = R^2\frac{\dot{s}^2}{s^2}\epsilon(2\tilde{U} - \tilde{M}). \tag{50}$$

Since $\epsilon \ll 1$, one can drop the last term on the left-hand side and then using expression (32) for ϵ we have

$$-K(r) = \frac{1}{r_0^2}(2\tilde{U} - \tilde{M}), \tag{51}$$

obtaining finally

$$\tilde{U} = \tfrac{1}{2}\big[\tilde{M} - K(r)r_0^2\big]. \tag{52}$$

In this equation the cancellation of ϵ gives a direct relation between $K(r)$ and the matter perturbations (tilde quantities). This is the only equation of the system where $K(r)$ appears explicitly. From the definition of Γ given by (15) one can rewrite (52) as

$$K(r) = \frac{1 - \Gamma^2}{r^2}. \tag{53}$$

This relation shows also the connection between the profile $K(r)$ and Γ.

Substituting (52) into equation (48) we get

$$\frac{\partial\tilde{M}}{\partial\xi} + \frac{5 + 3\gamma}{2}\tilde{M} = \frac{3}{2}(1 + \gamma)K(r)r_0^2, \tag{54}$$

and from this expression we can see that it is possible to separate the variables (r, ξ) because, as we have assumed at the beginning, γ is just a function of time. We therefore write

$$\tilde{M} = \Phi(\xi)K(r)r_0^2, \tag{55}$$

that gives the following differential equation for the function $\Phi(\xi)$

$$\frac{\mathrm{d}\Phi}{\mathrm{d}\xi} + \frac{5 + 3\gamma}{2}\Phi = \frac{3}{2}(1 + \gamma). \tag{56}$$

Expression (55) is the solution for the mass perturbation $\tilde{M}$ and inserting this into (49), (46) and (52) we obtain the following expressions for first order perturbations of energy density, $\tilde{e}$, lapse, $\tilde{a}$ and radial velocity, $\tilde{U}$:

$$\tilde{e} = \Phi(\xi)\frac{1}{3r^2}[r^3K(r)]'r_0^2 \tag{57}$$

$$\tilde{a} = -\Phi(\xi)\frac{\gamma}{1 + \gamma}\frac{1}{3r^2}[r^3K(r)]'r_0^2 \tag{58}$$

$$\tilde{U} = \frac{1}{2}[\Phi(\xi) - 1]K(r)r_0^2. \tag{59}$$

Substituting these equations into (44) and (45) we find two differential equations for $\tilde{R}$ and $\tilde{b}$, given by

$$(1 + 3\gamma)\tilde{R} + \frac{\partial\tilde{R}}{\partial\xi} = -\Phi(\xi)\frac{\gamma}{1 + \gamma}\frac{1}{3r^2}[r^3K(r)]'r_0^2 + \frac{1}{2}[\Phi(\xi) - 1]K(r)r_0^2, \tag{60}$$

$$(1 + 3\gamma)\tilde{b} + \frac{\partial\tilde{b}}{\partial\xi} = \frac{\gamma}{(1 + \gamma)}r\left[\frac{1}{3r^2}(r^3K(r))'\right]'\Phi(\xi), \tag{61}$$

that can be solved introducing two new functions of time $I_1(\xi)$ and $I_2(\xi)$ and writing

$$\tilde{R} = -I_1(\xi)\frac{1}{3r^2}[r^3K(r)]'r_0^2 + I_2(\xi)\frac{K(r)}{2}r_0^2, \tag{62}$$

$$\tilde{b} = I_1(\xi)r\left[\frac{1}{3r^2}(r^3K(r))'\right]'r_0^2. \tag{63}$$

The relations between $I_{1,2}(\xi)$ and $\Phi(\xi)$ are obtained by introducing (62) and (63) into (60) and (61):

$$\frac{\mathrm{d}I_1(\xi)}{\mathrm{d}\xi} + (1+3\gamma)I_1(\xi) = \frac{\gamma}{1+\gamma}\Phi(\xi) \tag{64}$$

$$\frac{\mathrm{d}I_2(\xi)}{\mathrm{d}\xi} + (1+3\gamma)I_2(\xi) = [\Phi(\xi) - 1]. \tag{65}$$

This completes the system of perturbation equations. It is worth mentioning that in these equations, time evolution is given by ϵ and Φ, while all of the spatial dependence is given by $K(r)$.

3. Perturbations in a multifluid medium

We assume that the universe consists of different perfect fluids characterized by different equations of state with different constants γ_i. For the unperturbed solution we can introduce an effective γ defined as

$$\gamma \equiv \frac{\sum_i p_i}{\sum_i e_i} = \frac{\sum_i \gamma_i e_i}{\sum_i e_i} = \frac{\sum_i \gamma_i e_i}{e}, \tag{66}$$

which in general is a function of time (however γ does not depend on time in the case of one single perfect fluid). At some moment of time t_0 (which is not necessarily the same moment when we impose the initial conditions) we specify the fractional contributions f_i of the different fluid components with the corresponding coefficients γ_i, having for each component

$$\frac{e_i}{e_{i0}} = \left(\frac{s}{s_0}\right)^{-3(1+\gamma_i)} \tag{67}$$

$$e_i = f_i e \tag{68}$$

$$\sum_i f_i = 1. \tag{69}$$

Using expressions (67) and (68) one can write

$$e_i = f_{i0}e_0\left(\frac{s}{s_0}\right)^{-3(1+\gamma)} \tag{70}$$

then from (66) and the equation of state (16) we have

$$\gamma = \frac{\sum_i f_{i0}\gamma_i s^{-3(1+\gamma_i)}}{\sum_i f_{i0}s^{-3(1+\gamma_i)}}. \tag{71}$$

Now we make the simplifying assumption that both the unperturbed and also the perturbed energy density and pressure are related by the effective equation of state $p = \gamma(t)e$. This

assumption is valid if the fractions f_i of the different fluids are homogeneous, i.e. they are the same in different places, varying only with time. In fact this assumption means that

$$\gamma \equiv \frac{p}{e} = \frac{p_b + \delta p}{e_b + \delta e} = \frac{p_b}{e_b},$$

where the right-hand side is obviously function of time only; hence δe and δp should satisfy the following condition

$$p_b \delta e - e_b \delta p = 0.$$

To the first order approximation this means that

$$\delta\left(\frac{p}{e}\right) = 0$$

or, in terms of f_i, we have

$$\delta\left(\frac{\sum_i \gamma_i \, \mathrm{e}_i}{e}\right) \equiv \delta\left(\sum_i \gamma_i f_i\right). \tag{72}$$

Taking into account that all γ_i are constants (which means $\delta\gamma_i = 0$), we can see that condition (72) is satisfied and hence the assumption $p = \gamma(t)e$ is valid if $\delta f_i = 0$. This assumption is obviously violated during a first order phase transition, if this transition takes place at different times in different places (i.e. it is inhomogeneous).

Let us now define a new quantity Q

$$Q(s) \equiv \sum_i f_{i0} s^{-3(1+\gamma_i)} \propto e(s). \tag{73}$$

Taking the time derivative of this quantity, one gets

$$\frac{\mathrm{d}Q}{\mathrm{d}\xi} = s\frac{\mathrm{d}Q}{\mathrm{d}s} = -3\sum_i (1+\gamma_i) f_{i0} s^{-3(1+\gamma_i)} = -3(1+\gamma)Q \tag{74}$$

and finally Q can be related to H_b by the following differential equation:

$$\frac{1}{2}\frac{\mathrm{d}Q}{Q\mathrm{d}\xi} = \frac{1}{H_b}\frac{\mathrm{d}H_b}{\mathrm{d}\xi}. \tag{75}$$

Inserting expressions (74) and (75) into (56) one obtains

$$\frac{\mathrm{d}\Phi}{\mathrm{d}\xi} + \left(1 - \frac{1}{H_b}\frac{\mathrm{d}H_b}{\mathrm{d}\xi}\right)\Phi = -\frac{1}{H_b}\frac{\mathrm{d}H_b}{\mathrm{d}\xi}. \tag{76}$$

The solution of this equation can be written in the form

$$\Phi = F\,\mathrm{e}^{\lambda},$$

where F and μ satisfy the following differential equations

$$\frac{\mathrm{d}F}{\mathrm{d}\xi} = -\frac{1}{H_b}\frac{\mathrm{d}H_b}{\mathrm{d}\xi}\mathrm{e}^{-\lambda}, \qquad \frac{\mathrm{d}\lambda}{\mathrm{d}\xi} + 1 - \frac{1}{H_b}\frac{\mathrm{d}H_b}{\mathrm{d}\xi} = 0,$$

which give

$$\mathrm{e}^{-\lambda} = \mathrm{e}^{\ln s - \ln H_b} = \frac{s}{H_b}, \qquad F = \frac{s}{H_b} - \int_0^s \frac{\mathrm{d}s}{H_b},$$

and finally

$$\Phi(s) = 1 - \frac{H_b(s)}{s}\int_0^s \frac{\mathrm{d}s}{H_b(s)}. \tag{77}$$

Now we can solve the two differential equations for I_1 and I_2 that are both of the same form,

$$s\frac{\mathrm{d}I_i(s)}{\mathrm{d}s} + (1+3\gamma)I_i(s) = F_i(s), \qquad i = 1, 2, \tag{78}$$

where $F_1(s) = \frac{\gamma(s)}{1+\gamma(s)}\Phi(s)$ and $F_2(s) = \Phi(s) - 1$. From the expression (33) we see that

$$1 + 3\gamma = \frac{1}{H_b\epsilon}\frac{\mathrm{d}\epsilon}{\mathrm{d}t} = H_b^2 s^2 \left(s\frac{d\left(1/H_b^2 s^2\right)}{\mathrm{d}s} \right) \tag{79}$$

and this allows the differential equations (78) to be written in a form that can easily be integrated,

$$s\frac{\mathrm{d}}{\mathrm{d}s}\left[\frac{1}{H_b^2 s^2} I(s)\right] = \frac{1}{H_b^2 s^2} F(s). \tag{80}$$

Then

$$I(s) = H_b^2(s)s^2 \int_0^s F(\tau)\frac{1}{H_b^2(\tau)}\frac{\mathrm{d}\tau}{\tau^3}, \tag{81}$$

which gives the following expressions for the two functions I_1 and I_2:

$$I_1(s) = H_b^2(s)s^2 \int_0^s \frac{\gamma(\tau)}{1+\gamma(\tau)}\Phi(\tau)\frac{1}{H_b^2(\tau)}\frac{\mathrm{d}\tau}{\tau^3}, \tag{82}$$

$$I_2(s) = H_b^2(s)s^2 \int_0^s (\Phi(\tau) - 1)\frac{1}{H_b^2(\tau)}\frac{\mathrm{d}\tau}{\tau^3}. \tag{83}$$

The initial conditions for all of the physical quantities have now been determined in a self-consistent way: the functions $Q(s)$ and $H_b(s)$ specify the multifluid medium consisting of different species of particles and fields (for example massive particles, photons, scalar fields, cosmic strings, etc) which are present in the universe, and hence in the configuration, at any time preceding the time chosen for imposing the initial conditions. In the particular case of a single fluid component, with $\gamma = \text{const}$, the functions Φ, I_1, and I_2 are also constants. We have in this case

$$H(s) \propto s^{-\frac{3(1+\gamma)}{2}}, \tag{84}$$

and

$$\Phi = \frac{3(1+\gamma)}{5+3\gamma} \tag{85}$$

$$I_1 = \frac{\gamma}{(1+3\gamma)(1+\gamma)}\Phi = \frac{3\gamma}{(1+3\gamma)(5+3\gamma)} \tag{86}$$

$$I_2 = \frac{1}{1+3\gamma}(\Phi - 1) = -\frac{2}{(1+3\gamma)(5+3\gamma)}. \tag{87}$$

Therefore in this simple case the tilde quantities are time independent and the time evolution is determined only by the parameter ϵ. From (33) we can calculate the time evolution of ϵ

$$\epsilon(t) \propto \left(\frac{t}{t_0}\right)^{\frac{2(1+3\gamma)}{3(1+\gamma)}}, \tag{88}$$

which is the same as the standard solution for a growing mode in cosmological perturbation theory (see for example [31, 32]).

4. General properties of the curvature profile

From the definition of b given by (39) we obtain the obvious mathematical requirement

$$1 - K(r)r^2 > 0 \quad \Rightarrow \quad K(r) < \frac{1}{r^2}. \tag{89}$$

This corresponds to the physical condition that a perturbed spherical region of comoving radius r should not be causally disconnected from the rest of the universe. This condition was formulated in [33] and recently analysed in [34], where the perturbation was described by a region with $K = 1$, embedded in a region with $K = 0$.

Another important requirement is related to the causality principle (see [6]) and is given by condition that the total excess of mass in the initial configuration should be equal to zero

$$\int_0^\infty 4\pi r^2 \tilde{e}(r)\, \mathrm{d}r = 0. \tag{90}$$

As follows from (57) this is equivalent to

$$\lim_{r\to\infty} r^3 K(r) = 0. \tag{91}$$

Condition (90) follows from conservation of total mass–energy and is related to the fact that we consider in the present paper only local configurations within spatially flat universe. This requirement is related with the causality principle in the following way. Let us consider an observer A situated far away from the initial configuration. The causality principle says that the observer A cannot 'know' about the existence of the configuration unless some signal, e.g. an acoustic wave, has enough time to reach A. Violation of the causality principle in this context means that, if condition (90) is not satisfied, A could experience gravitational attraction by the configuration and hence could 'know' about its existence before any physical signal could reach A.

An important parameter characterizing the curvature profile is the value of r_0 that specifies the comoving length scale of the overdense region in the configuration. From (57) we have

$$\tilde{e}(r_0) = 0 \quad \Rightarrow \quad K(r_0) + \frac{r_0}{3} K'(r_0) = 0. \tag{92}$$

It is useful to introduce an integrated quantity δ that measures the mass excess inside the overdense region, as frequently done in literature. From equation (57), one can see that any spherical integral of $\tilde{e}$ does not depend on the particular curvature profile used, but depends only on the value of $K(r)$ at the outer edge of the configuration. The expression for δ in terms of the curvature profile is then given by

$$\delta \equiv \left(\frac{4}{3}\pi r_0^3\right)^{-1} \int_0^{r_0} 4\pi \frac{e - e_b}{e_b} r^2\, \mathrm{d}r = \epsilon(s)\Phi(s)K(r_0)r_0^2. \tag{93}$$

5. Parametrization of the curvature profile

In this section we specify the profile $K(r)$ in terms of two free parameters. It is natural to start with a centrally peaked profile of the energy density, such that outside the overdense region there is an under-dense region which then becomes asymptotically flat. To obtain an energy density profile with these properties, one should choose a centrally peaked curvature profile which is described in terms of a suitable continuous function and tends asymptotically to zero as $r \to \infty$. Continuity should be ensured at least in the first and second derivatives, because these derivatives play a crucial role in the expressions for the perturbation profiles

of density and velocity. We put $K(0) = 1$, using the same normalization as in the case of a closed universe.

We start with a family of curvature profiles based on a Gaussian shape, described by

$$K(r) = \left(1 + \alpha \frac{r^2}{2\Delta^2}\right) \exp\left(-\frac{r^2}{2\Delta^2}\right), \tag{94}$$

where α and Δ are two independent parameters. In the particular case $\alpha = 0$, the profile $K(r)$ is exactly Gaussian. The first derivative of $K(r)$ is given by

$$K'(r) = \frac{r}{\Delta^2}\left[\alpha - \left(1 + \alpha \frac{r^2}{\Delta^2}\right)\right] \exp\left(-\frac{r^2}{2\Delta^2}\right), \tag{95}$$

and we use this to calculate the value of r_0 as a function of α and Δ using (94) and (92). We obtain a quadratic equation with the following solutions for r_0:

$$r_0^2 = 3\Delta^2 \qquad \text{if} \qquad \alpha = 0 \tag{96}$$

$$r_0^2 = \Delta^2 \frac{(5\alpha - 2) + \sqrt{(5\alpha - 2)^2 + 24\alpha}}{2\alpha} \qquad \text{if} \qquad \alpha \neq 0 \tag{97}$$

that we substitute into (35) to express the spatial comoving coordinate r in terms of the background coordinate R_b. It is then convenient to express r_0 in terms of the initial perturbation length scale R_0. We therefore introduce a dimensionless ratio of the circumferential radius to R_0 defined as $Z \equiv R_b/R_0$, which is equal to 1 at the edge of the overdense region. Thus the exponential argument in (94) is given by

$$\frac{r^2}{\Delta^2} = \frac{F(\alpha)}{2\alpha} Z^2, \tag{98}$$

where

$$F(\alpha) \equiv (5\alpha - 2) + \sqrt{(5\alpha - 2)^2 + 24\alpha} \qquad \text{if} \qquad \alpha \neq 0 \tag{99}$$

$$\frac{F(\alpha)}{\alpha} = 3 \quad \text{if} \quad \alpha = 0 \tag{100}$$

and one can see that the parameter Δ cancels in the expression for r/r_0, making clear the physical meaning of α and Δ: for the energy density perturbation profile expressed in terms of Z we get

$$\tilde{e}(Z) = \Phi(\xi) \frac{\Delta^2}{2\alpha} F(\alpha) \left[1 + \left(\frac{5}{6}\alpha - 1\right) \frac{F(\alpha)}{2\alpha} Z^2 - \frac{\alpha}{2}\left(\frac{F(\alpha)}{2\alpha}\right)^2 Z^4\right] \exp\left(-\frac{F(\alpha)}{4\alpha} Z^2\right) \tag{101}$$

and we see that the spatial profile given by the expression inside the parentheses depends only on α. Hence Δ, appearing only outside the brackets, parametrizes the amplitude of the density perturbation. The separation of factors in (101) allows us to control the values of the input parameters independently.

The value of the second derivative of $K(r)$ at the centre is given by

$$K''(0) = \frac{\alpha - 1}{\Delta^2}. \tag{102}$$

When $\alpha > 1$, $K''(0)$ is positive and an off-centred peak appears in the profiles of both curvature and energy density. For $\alpha < 0$, there is a second overdense region, corresponding to a second solution for r_0. Because we are interested in solutions that represent perturbations centred at

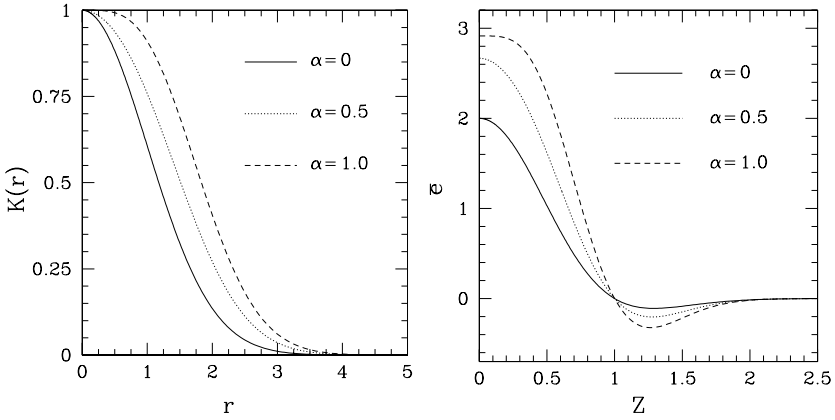

Figure 1. The left-hand plot shows the curvature profile $K(r)$ as a function of the comoving coordinate for three different values of α (0, 0.5 and 1). The right-hand plot shows the corresponding profiles of the energy density perturbation $\tilde{e}$ plotted as functions of Z. These cases and those described in the next figures have been calculated with $\gamma = 1/3$ (equivalent to $\Phi = 2/3$).

$r = 0$ surrounded by an underdense region which becomes asymptotically flat, we restrict our attention to the range of shapes given by $0 \leqslant \alpha \leqslant 1$.

In figure 1 we plot corresponding curvature and energy density profiles for three different values of α between 0 and 1, keeping the same value of Δ.

The particular case with $\alpha = 0$ in (101) coincides with one of the profiles used in [19, 25]:

$$\tilde{e}(Z) = \Delta^2 \left[1 + \frac{3}{2}Z^2\right] \exp\left(-\frac{3}{2}Z^2\right), \tag{103}$$

where the parameter Δ has the same meaning as the quantity used in [19, 25] to parametrize the amplitude of the density perturbation.

An advantage of the present description is the possibility of calculating the perturbation amplitude δ, defined in (93), directly from the curvature profile. Using (103) for an arbitrary value of α we have

$$\delta = \frac{1}{3N^2}\frac{\Delta^2}{\alpha}F(\alpha)\left(1 + \frac{F(\alpha)}{4}\right)\exp\left(-\frac{F(\alpha)}{4\alpha}\right). \tag{104}$$

Applying condition (89) we calculate the maximum allowed value of δ and then we obtain the corresponding maximum value of Δ for each α. The results of these calculations are presented in figure 2 for two different cases ($\alpha = 0$ and $\alpha = 1$). From these plots, we can see that for wider curvature profiles, corresponding to larger values of Δ we have energy density profiles with higher central amplitude. This corresponds to larger values of the perturbation amplitude δ defined in (93).

Next we consider another parametrization of curvature that allows us to work with curvature profiles with a sharper transition from $K = 1$ to $K = 0$. The new parametrization is given by the following expression:

$$K(r) = \begin{cases} 1 & \text{if} \quad r \leqslant \Delta_* \\ \left(1 + \dfrac{(r-\Delta_*)^2}{2\Delta^2}\right)\exp\left(-\dfrac{(r-\Delta_*)^2}{2\Delta^2}\right) & \text{if} \quad r > \Delta_* \end{cases} \tag{105}$$

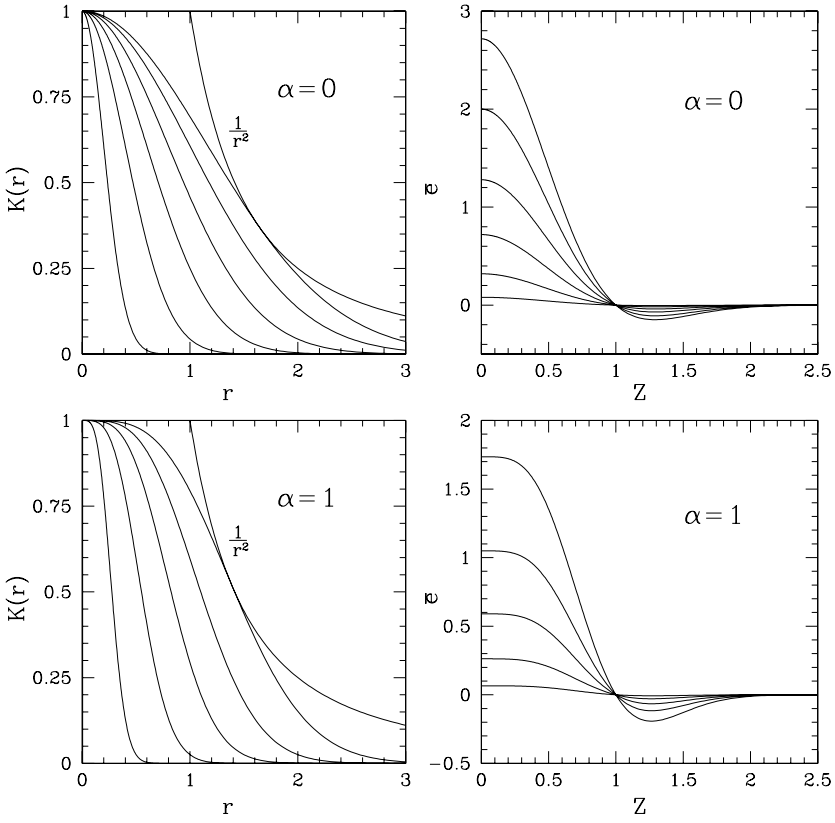

Figure 2. The left-hand plots show the curvature profiles $K(r)$ as functions of the comoving coordinate r, while the right-hand plots show the corresponding profiles for the energy density perturbations $\tilde{e}$ plotted as functions of Z. For $\alpha = 0$ (upper plots) the different profiles correspond to Δ between 0.2 and 1.16, which is the maximum value allowed by (89). The values of Δ are higher for the higher curves. For $\alpha = 1$ (lower plots), the values of Δ used are between 0.15 and 0.77.

and its first derivative is

$$K'(r) = \begin{cases} 0 & \text{if} \quad r \leqslant \Delta_* \\ -\dfrac{(r-\Delta_*)^3}{2\Delta^4} \exp\left(-\dfrac{(r-\Delta_*)^2}{2\Delta^2}\right) & \text{if} \quad r > \Delta_* \end{cases}. \tag{106}$$

In figure 3 we present the parametrization given by (105), indicating explicitly the two independent parameters Δ and Δ_*: Δ_* specifies the radius of the plateau with $K(r) = 1$, Δ describes the sharpness of the transition region. In particular, when $\Delta_* = 0$ the curvature profile coincides with the previous case for $\alpha = 1$. Applying condition (92) we obtain a quadratic equation to calculate the value of r_0, that we solve numerically using the Newton–Raphson method [35]. The maximum value of Δ_* satisfying condition (89) is 1, while the minimum value of δ, obtained when $\Delta = 0$, is $\delta_{\min} = 2\Delta_*^2/3N^2$.

In figure 4, the top-left plot shows the dependence of $K(r)$ on Δ with Δ_* kept fixed, while the bottom-left plot shows the dependence of $K(r)$ on Δ_* with Δ kept fixed. In the right-hand

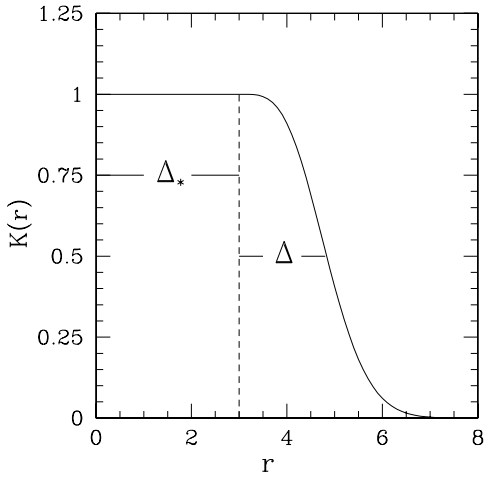

Figure 3. This figure shows the behaviour of $K(r)$ given by (105), indicating explicitly the meaning of the two parameters Δ and Δ_*.

plots, we show the corresponding profiles of $\tilde{e}(r)$. As in figure 2, wider curvature profiles correspond to density profiles with a higher central amplitude.

6. Numerical tests and calculations

6.1. Numerical tests

Next we discuss the numerical tests performed so as to be confident that the perturbation profile $K(r)$ has been introduced consistently into the code. For this we analysed the accuracy of our first order approach (first order with respect to $\epsilon = 1/N^2$). In other words, imposing a perturbation with a length scale much larger than the cosmological horizon r_H, we checked whether ϵ is small enough to make higher order terms negligible. A first requirement for a satisfactory value of N is that the comoving length scale of the horizon r_H should be sufficiently smaller than the sharpness Δ of the curvature profile. This means that $r_H \ll \Delta$. From equation (35), $r_H = r_0/N$ which then gives the condition,

$$N \gg \frac{r_0}{\Delta}. \tag{107}$$

Using the curvature profile given by (94) we have $r_0 \simeq \Delta$ for $0 \leqslant \alpha \leqslant 1$, while for the curvature profile given by (105) we have that $r_0 \simeq \Delta_* + \Delta$. Substituting these two relations into (107), we see that both conditions are satisfied if

$$N \gg 1 + \frac{\Delta_*}{\Delta}. \tag{108}$$

This expression is valid also for the curvature profile given by (94) if we put $\Delta_* = 0$. From this expression we can see that a sharper profile, with $\Delta_*/\Delta \gg 1$, requires larger values of N.

For each set of initial input parameters we made several numerical tests. Here we present four sample cases that demonstrate how these tests work. The main test is based on equation (53), which is used to rederive $K(r)$ after calculating the initial conditions for the various quantities. Expression (53) is valid when the higher order terms are negligible and so

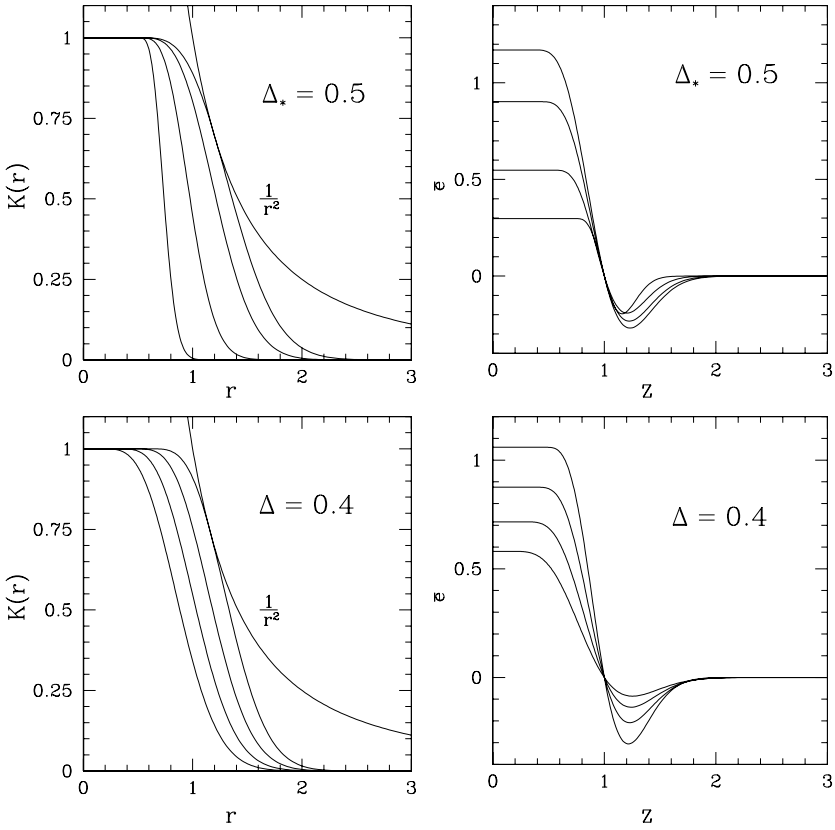

Figure 4. The left-hand plots show the curvature profile $K(r)$ for Δ_* constant and varying Δ (top row) and for Δ constant and varying Δ_* (bottom row). The corresponding behaviour of the energy density perturbation $\tilde{e}$ is shown in the right-hand plots.

we expect to find some difference between the profiles of $K(r)$ calculated with (53) and the original ones introduced analytically to describe the initial conditions. In figure 5 we plot the result of this test using $K(r)$ given by (94), with $\alpha = 0$ on the left and $\alpha = 1$ on the right. In figure 6 we plot $K(r)$ given by (105), using the ratio Δ_*/Δ equal to 1 in the left panel, and equal to 20 in the right panel. In all of these plots the solid line shows the analytical profile of $K(r)$, while the dashed lines correspond to the profiles of $K(r)$ calculated with (53) using different values of N. The first value used was $N = 1$ (which we know is not large enough, and this is also clear from the plots) and then we increased N. In the first three cases, corresponding to curvature profiles with $\Delta_*/\Delta \leqslant 1$, we found that $N = 10$ is large enough to achieve acceptable precision. In the last case, when $\Delta_*/\Delta = 20$, we found that $N = 25$ is sufficiently large. Because we did not see any significant difference between the analytical and numerical values of $K(r)$, for the highest values of N plotted in figure 5 and 6 we assume that these values of N are satisfactory. To be more certain of this we also made another test, analysing numerically the evolution of configurations corresponding to the curvature profiles $K(r)$ presented in figures 5 and 6. We have verified that the values of N indicated by the previous test do give essentially the same numerical evolution as for larger values of N (a standard test for numerical computations).

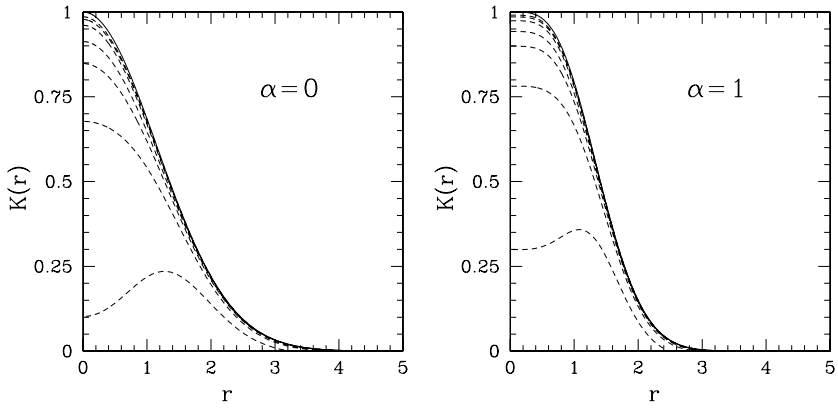

Figure 5. These plots show the comparison between the analytical curvature profiles (solid line) and the numerical curvature profiles (dashed line) given by (94). The different dashed lines correspond to $N = 1, 2, 3, 4, 6, 8, 10$ with the higher curves corresponding to the higher values of N. The profiles in the left-hand plot for ($\alpha = 0$, $\Delta = 1.15$), and the profiles in the right-hand plot are for ($\alpha = 1$, $\Delta = 0.77$).

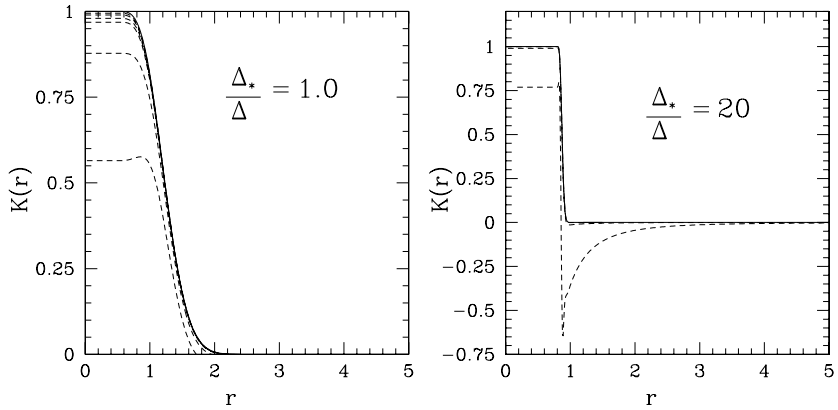

Figure 6. These plots show the comparison between the analytical curvature profiles (solid line) and the numerical curvature profiles (dashed lines) given by (105). The different dashed lines correspond to $N = 1, 2, 4, 5, 7, 10$ in the left plot and $N = 1, 5, 25$ in the right one, with the higher curves corresponding to the higher values of N. The profiles in the left-hand plot are for $\Delta_*/\Delta = 1$, and the profiles in the right-hand plot are for $\Delta_*/\Delta = 20$.

To complete our tests we used the constraint equation (15) for convergence test to estimate the precision of the code. The measured convergence is of roughly second order as expected from the form of the difference scheme being used. For the number of gridpoints used in the simulations presented here, the accuracy of the code is better than one part in 10^4.

6.2. Description of the calculations

The calculations of black hole formation performed with initial conditions specified in terms of a curvature profile, show similar hydrodynamical features as those presented in [25], where the same numerical technique was used. We present here four sample cases: two correspond to

black hole formation, where the observer time slicing has been used, and two correspond to no black hole formation, where we have used the cosmic time slicing. Each case is characterized by a particular value of the density perturbation amplitude δ and it is useful to introduce at this stage a measure of δ which is independent of the initial scale used when imposing the initial conditions. Looking at expression (93), we can see that in the case of constant γ, if we define $\tilde{\delta} \equiv N^2\delta$, the expression becomes time independent, giving in the radiation epoch

$$\tilde{\delta} = \tfrac{2}{3}K(r_0)r_0^2. \tag{109}$$

Comparing this value with the value of δ at horizon crossing, we find that it is of the same order (with a small correction due to the nonlinear growth of the energy density near to horizon crossing). Therefore for the rest of the discussion we use $\tilde{\delta}$ as the amplitude of density perturbations. The dividing line between perturbations that collapse to form black holes and perturbations that disperse into the background is characterized by a threshold amplitude $\tilde{\delta}_c$. This value was estimated numerically by making a converging sequence of numerical calculations until a satisfactory precision in determination of $\tilde{\delta}_c$ was achieved.

The observer time coordinate u is defined by

$$f\,\mathrm{d}u = a\,\mathrm{d}t - b\,\mathrm{d}r, \tag{110}$$

where f is the lapse in the new coordinate system. The metric is then

$$\mathrm{d}s^2 = -f^2\,\mathrm{d}u^2 - 2fb\,\mathrm{d}r\,\mathrm{d}u + R^2(\mathrm{d}\theta^2 + \sin^2\theta\,\mathrm{d}\phi^2). \tag{111}$$

When using observer-time slicing, black hole formation occurs when both the lapse f and $\Gamma + U$ tend to zero (see [25]). These conditions are reached asymptotically and correspond to the formation of an apparent horizon, seen by a distant observer as having an infinite redshift. When using observer-time slicing, black hole formation occurs when both the lapse f and $\Gamma + U$ tend to zero (see [25]). These conditions are reached asymptotically and correspond to the formation of an apparent horizon, seen by an outside observer as having infinite redshift. The observer time u is scaled so as to synchronize with proper time as measured by a standard FRW fundamental observer located at the outer edge of the grid, beyond the range of influence of the perturbation. This scaling is achieved by setting $f = 1$ at the outer edge of the grid.

We illustrate the two examples of black hole formation, shown in figures 7 and 8, by plotting profiles of the radial velocity U, lapse f, the $2M/R$ ratio and the mass M as functions of the circumferential radius R at the initial time, an intermediate time and a final time, labelled as u_0, u_i and u_f, respectively. Figures 7 and 8 show the formation of black holes for two different values of $(\tilde{\delta} - \tilde{\delta}_c)$ with the smaller value giving rise to the lower mass black hole as expected [6, 19, 25, 36].

The upper left-hand plots of these two figures show the behaviour of the radial velocity U. Here the time sequence starts from the top curve and continues towards the bottom one. Note that, after a certain time U becomes negative in the central regions, and that the apparent horizon (where $2M/R \to 1$) forms at the minimum of the radial velocity profile. Outside this region there is first an intermediate shell with negative velocity corresponding to matter accreting into the black hole, then there is a region of positive velocity corresponding to the rest of the expanding universe.

The upper right-hand plots show the behaviour of the lapse function f with the time sequence of the curves given by the decreasing central value of f. One can see that a plateau forms in the central region, where the black hole is forming, and that the lapse tends asymptotically to zero there. The 'freezing' of the evolution, as mentioned above, is one of the fundamental criteria for black hole formation. The other important feature of black hole formation is the trapped surface condition ($\Gamma + U \to 0$) which corresponds to $2M/R \to 1$.

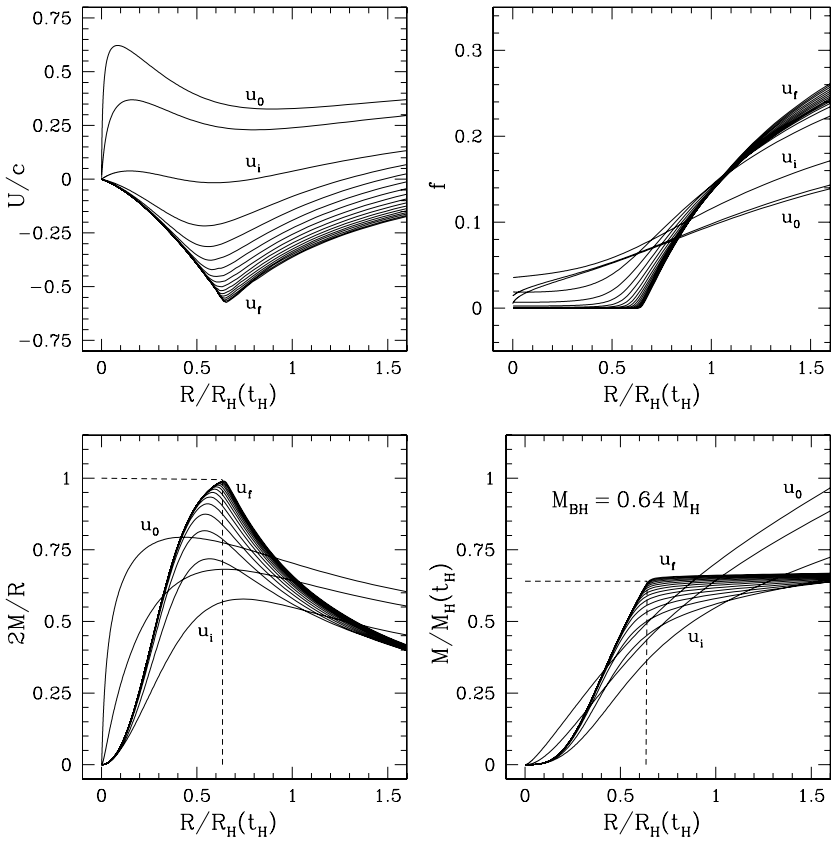

Figure 7. A typical evolution leading to black hole formation: the initial curvature profile used is characterized by $\alpha = 0$ and $\Delta = 1.02$, which give $(\tilde{\delta} - \tilde{\delta}_c) = 1.3 \times 10^{-2}$. The upper plots show the profile of radial velocity U/c and lapse f at different times, while the bottom panels show the corresponding profiles of $2M/R$ and mass M. Here u_0, u_i and u_f are respectively the initial, intermediate and final times.

In the bottom left-hand plots, $2M/R$ is shown asymptotically tending to 1 at the maximum of the curve. This determines the location where the apparent horizon will form. In this case the time sequence of the curves is given at first by the decreasing values of $2M/R$ at the right edge of the plot, and then by the increasing of the maximum of these curves towards 1.

Finally the bottom right-hand plots show the corresponding behaviour of the mass M, indicating the value of the mass of the black hole formed. At late times, one sees the convergence of the curves. In figures 7 and 8 the circumferential radius R and mass M have been normalized with respect to the values for the cosmological horizon scale at the horizon crossing time.

Results from two representative calculation with $\tilde{\delta} < \tilde{\delta}_c$ (using cosmic time) are shown in figure 9, where we have plotted the energy density normalized with respect to the current background value, as a function of $R/R_H(t_i)$. The left-hand plot corresponds to a small curvature perturbation far from the threshold $\tilde{\delta}_c$ with $\tilde{\delta} = 4.46 \times 10^{-3}$ and $(\tilde{\delta} - \tilde{\delta}_c) = -0.45$. In this case negative velocities are never reached: initially, the expansion of the central region proceeds more slowly than the expansion of the background. After

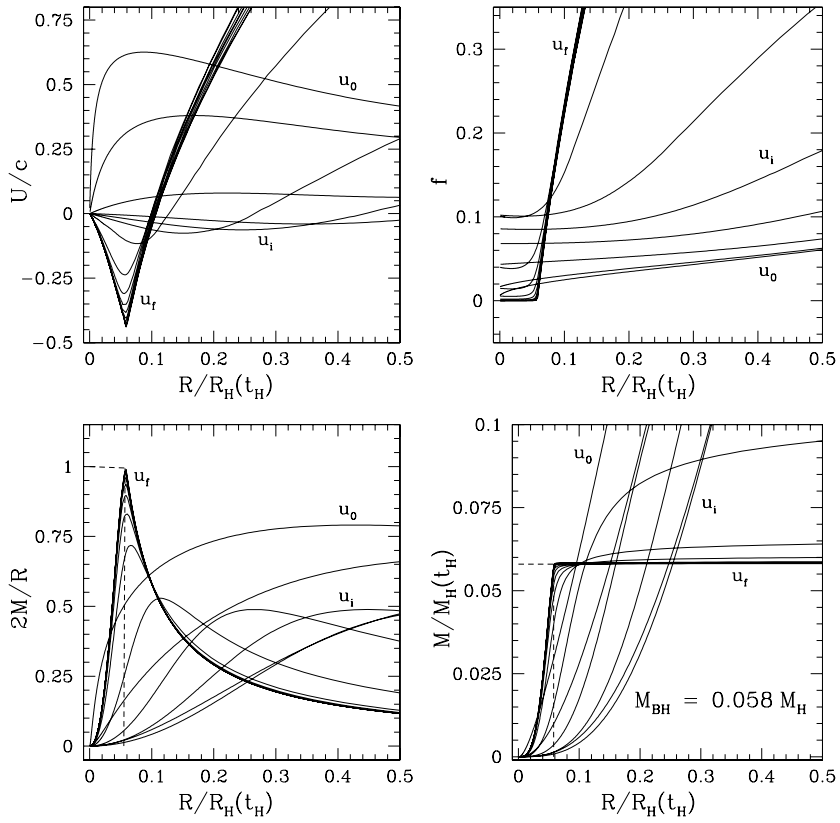

Figure 8. A typical evolution leading to black hole formation: the initial curvature profile used is characterized by $\Delta_* = 0.8$ and $\Delta = 0.18$, which give $(\tilde{\delta} - \tilde{\delta}_c) = 1.8 \times 10^{-3}$. The upper plots show the profile of radial velocity U/c and lapse f at different times, while the bottom panels show the corresponding profiles of $2M/R$ and mass M. Here u_0, u_i and u_f are respectively the initial, intermediate and final times.

horizon crossing, the perturbation is damped and a compression wave propagates outwards through the expanding medium. The other example shown in the right-hand plot is for a case with $(\tilde{\delta} - \tilde{\delta}_c) = -2.67 \times 10^{-2}$. In this case the perturbation amplitude $\tilde{\delta} = 0.49$ is close enough to $\tilde{\delta}_c = 0.52$ to give rise to an initial collapse of the central region. Because the gravitational potential is not large enough to form a trapped surface, as happens when $\tilde{\delta} > \tilde{\delta_c}$, the collapsing matter bounces producing a compression wave which expands outwards. These hydrodynamical features were first seen in [6] and were then analysed in detail in [25].

As a final result of these computations we determined the parameter ranges corresponding to black hole formation for the curvature profiles given by (94) and (105). Figure 10 summarizes the results. The left-hand plot shows the results obtained for different values of Δ and α used in parametrization (94), with the plane being divided into three different regions: the first corresponds to no black hole formation, the second to black hole formation and the third one to disconnected configurations $(K(r)r^2 \geqslant 1)$. It can be seen that the region of parameters corresponding to black-hole formation is quite narrow.

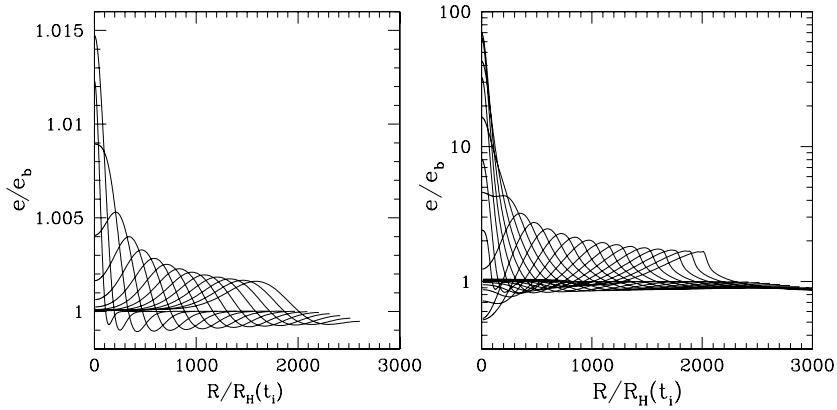

Figure 9. The left-hand plot shows a typical evolution of the energy density profile of a perturbation with $\tilde{\delta} \ll \tilde{\delta}_c$. In this case we have used expression (94) with $\alpha = 0, \Delta = 0.1$ and $N = 10$, corresponding to $\tilde{\delta} = 4.6 \times 10^{-3}$. The right-hand plot shows the typical evolution of a collapse when $\tilde{\delta} \lesssim \tilde{\delta}_c$. In this case we have used expression (105) with $\Delta_* = 0.5$, $\Delta = 0.37$ and $N = 10$, corresponding to $\tilde{\delta} = 0.49$.

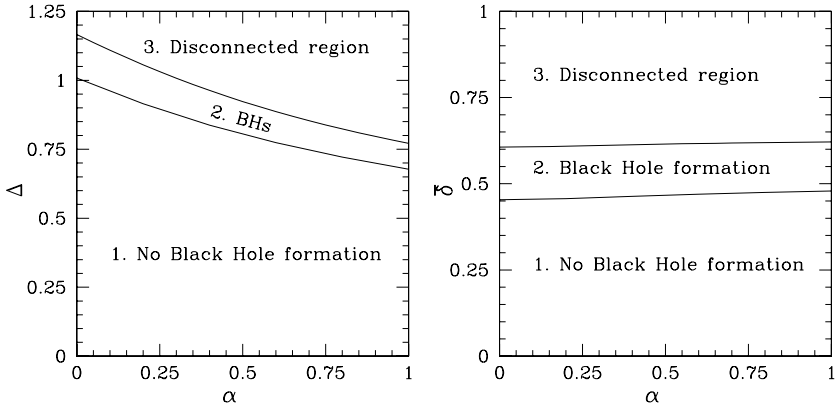

Figure 10. These plots show which values of α, Δ and $\tilde{\delta}$ lead to black hole formation or to an initial perturbation already disconnected from the rest of the universe for the case of $K(r)$ given by expression (94).

The same results are presented in terms of $\tilde{\delta}$ and α in the right-hand plot of figure 10. This shows very weak dependence of δ_c and $\delta_{\max}$ on α. We found that $\tilde{\delta}_c \simeq 0.45$, $\tilde{\delta}_{\max} \simeq 0.60$ for $\alpha = 0$ and $\tilde{\delta}_c \simeq 0.47$, $\tilde{\delta}_{\max} \simeq 0.62$ for $\alpha = 1$.

In figure 11 we present similar results for the second curvature parametrization given by (105). The left-hand plot shows the parameter space for Δ and Δ_*, and one can see the same three regions in the left-hand plot as in figure 10. The right-hand plot shows the same results in terms of Δ_* and $\tilde{\delta}$.

For the wide range of parameters explored so far, giving black hole masses down to 10^{-2} times the horizon mass, we have not yet seen any formation of shocks as had been seen in some earlier works [6, 19, 25, 36]. This is an important issue and work is in progress to investigate it more systematically.

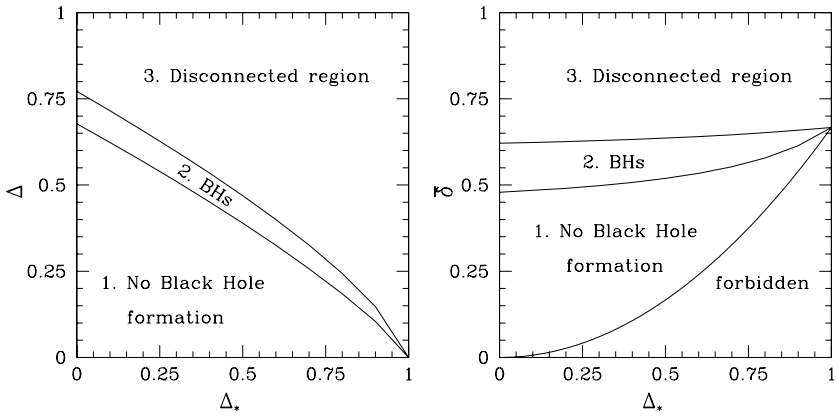

Figure 11. These plots show the range of parameters Δ, Δ_* and $\tilde{\delta}$ giving rise to black hole formation for the case of $K(r)$ given by (105).

7. Conclusion

Using the quasi-homogeneous solution, we have imposed initial conditions for PBH formation by introducing a time-independent curvature profile $K(r)$. This profile is the only source of perturbations in the fluid quantities and those perturbations behave as pure growing modes. We have obtained an analytical solution of the Misner–Sharp system of equations expressing initial perturbations of density and velocity in terms of the curvature profile $K(r)$ in the rather general case where matter in the universe can be treated as an arbitrary mixture of perfect fluids. We have performed numerical calculations for $\gamma = 1/3$ to test the self-consistency of these initial conditions for two different parametrizations of $K(r)$. Specifying the initial conditions using a curvature profile seems to be an improvement in the analysis of the PBH formation scenario since it allows initial conditions for all of the hydrodynamical variables relevant for the problem to be specified in self-consistent way.

We have shown that, in agreement with [6], the formation of PBHs requires higher amplitudes of strong metric deviation for sharper profiles of $K(r)$. Thus the Gaussian curvature profile, which is the least sharp, is the most favourable for PBH formation. For this case we found $\delta_c \simeq 0.45$ in agreement with [25]. The comparison of results obtained for the two different parametrizations of curvature profiles has shown that the shape of the initial profile plays crucial role for PBH formation. This is an important reason to calculate the probability for having different curvature profiles (work in progress) [37] and to link this probability with statistics of PBHs. Such a link should greatly improve the constraints on possible cosmological models obtained from observational upper limits on PBHs.

Acknowledgments

In the course of this work, we have benefited from helpful discussions with many colleagues including John Miller, Bernard Carr, Pavel Ivanov, Luciano Rezzolla and Carlo Baccigalupi.

Appendix A. Scalar curvature

In this appendix we express the scalar curvature in terms of the curvature profile $K(r)$. The general spherically symmetric metric in the cosmic time coordinate is

$$\mathrm{d}s^2 = -a^2\,\mathrm{d}t^2 + b^2\,\mathrm{d}r^2 + R^2\,\mathrm{d}\Omega^2, \tag{A.1}$$

where the metric tensor $g_{\alpha\beta}$ is diagonal and a, b and R are, in general, functions of r and t. The Christoffel symbols are calculated from

$$\Gamma^{\alpha}_{\beta\gamma} = \frac{1}{2}g^{\alpha\alpha}\left(\frac{\partial g_{\beta\alpha}}{\partial x^{\gamma}} + \frac{\partial g_{\gamma\delta}}{\partial x^{\beta}} - \frac{\partial g_{\beta\gamma}}{\partial x^{\delta}}\right), \tag{A.2}$$

while the components of the Ricci Tensor are given by

$$R_{\alpha\beta} = \Gamma^{\gamma}_{\delta\gamma}\Gamma^{\delta}_{\alpha\beta} - \Gamma^{\gamma}_{\delta\beta}\Gamma^{\delta}_{\alpha\gamma} + \frac{\partial\Gamma^{\gamma}_{\alpha\beta}}{\partial x^{\gamma}} - \frac{\partial\Gamma^{\gamma}_{\alpha\gamma}}{\partial x^{\beta}} \tag{A.3}$$

and to calculate the scalar curvature we need to take into account only the diagonal components $R_{\alpha\alpha}$.

In the background universe with the FRW metric the metric components are

$$a = 1 \qquad b = \frac{s(t)}{\sqrt{1 - Kr^2}} \qquad R = s(t)r, \tag{A.4}$$

where the curvature K is a constant equal to $0, \pm 1$. The diagonal components of the Ricci tensor are

$$R_{00} = 3\frac{\ddot{s}}{s} \tag{A.5}$$

$$R_{11} = \frac{s\ddot{s} + 2\dot{s}^2 + 2K}{1 - Kr^2} \tag{A.6}$$

$$R_{22} = (s\ddot{s} + 2\dot{s} + 2K)r^2 \tag{A.7}$$

$$R_{33} = R_{22}\sin^2\theta \tag{A.8}$$

and these are used to calculate the scalar curvature

$$R = 6\left(\frac{\ddot{s}}{s} + \frac{\dot{s}^2}{s^2} + \frac{K}{s^2}\right). \tag{A.9}$$

The 3-curvature is obtained by removing the terms with time derivatives, giving

$$R^{(3)} = 6\frac{K}{s^2}. \tag{A.10}$$

In the general case of the metric given by equation (A.1), the diagonal components of the Ricci tensor are

$$R_{00} = \frac{1}{a}\frac{\partial a}{\partial t}\left(\frac{1}{b}\frac{\partial b}{\partial t} + \frac{2}{R}\frac{\partial R}{\partial t}\right) + \frac{a}{b^2}\frac{\partial a}{\partial r}\left(\frac{2}{R}\frac{\partial R}{\partial r} - \frac{1}{b}\frac{\partial b}{\partial r}\right) + \frac{a}{b^2}\frac{\partial^2 a}{\partial r^2} - \frac{1}{b}\frac{\partial^2 b}{\partial t^2} - \frac{2}{R}\frac{\partial^2 R}{\partial t^2} \tag{A.11}$$

$$R_{11} = \frac{b}{a^2}\frac{\partial b}{\partial t}\left(\frac{2}{R}\frac{\partial R}{\partial t} - \frac{1}{a}\frac{\partial a}{\partial t}\right) + \frac{1}{b}\frac{\partial b}{\partial r}\left(\frac{1}{a}\frac{\partial a}{\partial r} + \frac{2}{R}\frac{\partial R}{\partial r}\right) + \frac{b}{a^2}\frac{\partial^2 b}{\partial t^2} - \frac{1}{a}\frac{\partial^2 a}{\partial r^2} - \frac{2}{R}\frac{\partial^2 R}{\partial r^2} \tag{A.12}$$

$$R_{22} = \frac{R}{a^2}\frac{\partial R}{\partial t}\left(\frac{1}{b}\frac{\partial b}{\partial t} - \frac{1}{a}\frac{\partial a}{\partial t}\right) + \frac{R}{b^2}\frac{\partial R}{\partial r}\left(\frac{1}{b}\frac{\partial b}{\partial r} - \frac{1}{a}\frac{\partial a}{\partial r}\right) + \left(\frac{1}{a}\frac{\partial R}{\partial t}\right)^2 - \left(\frac{1}{b}\frac{\partial R}{\partial r}\right)^2 + R\left(\frac{1}{a^2}\frac{\partial^2 R}{\partial t^2} - \frac{1}{b^2}\frac{\partial R}{\partial r^2}\right) + 1 \tag{A.13}$$

$$R_{33} = R_{22}\sin^2\theta. \tag{A.14}$$

Then we get

$$R = 2\left[\frac{D_t^2 b}{b} + 2\frac{D_t^2 R}{R} - \frac{D_r^2 a}{a} - 2\frac{D_r^2 R}{R} + \left(\frac{D_t R}{R}\right)^2 - \left(\frac{D_r R}{R}\right)^2 + 2\frac{D_t b}{b}\frac{D_t R}{R} - 2\frac{D_t a}{a}\frac{D_t R}{R} - \frac{D_t a}{a}\frac{D_t b}{b} + 2\frac{D_r b}{b}\frac{D_r R}{R} + \frac{D_r a}{a}\frac{D_r b}{b} - 2\frac{D_r a}{a}\frac{D_r R}{R} + \frac{1}{R^2}\right], \tag{A.15}$$

where the following operators have been defined:

$$D_t \equiv \frac{1}{a}\frac{\partial}{\partial t}, \qquad D_t^2 \equiv \frac{1}{a^2}\frac{\partial^2}{\partial t^2}, \qquad D_r \equiv \frac{1}{b}\frac{\partial}{\partial r}, \qquad D_r^2 \equiv \frac{1}{b^2}\frac{\partial^2}{\partial r^2}. \tag{A.16}$$

Substituting the expressions for a, b and R given by equations (35), (39), (40), expressing $\tilde{a}, \tilde{b}, \tilde{R}$ in terms of $K(r)$ and using equation (33), we find that the scalar curvature is given by

$$R = \left[6\frac{\ddot{s}}{s}\left(1 + \epsilon\frac{3\gamma - 1}{5 + 3\gamma}\mathcal{K}\right) + \frac{\dot{s}^2}{s^2}\left(1 - \epsilon\frac{2(2 + 3\gamma)}{5 + 3\gamma}\mathcal{K}\right) + \frac{\mathcal{K}}{s^2}\right], \tag{A.17}$$

where

$$\mathcal{K} = K(r) + \frac{r}{3}K'(r). \tag{A.18}$$

Comparing equation (A.17) with equation (A.9) we can see how the scalar curvature R is related to the curvature profile $K(r)$.

References

[1] Zel'dovich Ya B and Novikov I D 1966 *Astron. Zh.* **43** 758
Zel'dovich Ya B and Novikov I D 1967 *Sov. Astron.* **10** 602
[2] Hawking S W 1971 *Mon. Not. R. Astron. Soc.* **152** 75
[3] Carr B J 2003 *Lecture Notes Phys.* **631** 301
[4] Hawking S W 1974 *Nature* **248** 30
[5] Carr B J 1975 *Astrophys. J.* **201** 1
[6] Nadezhin D K, Novikov I D and Polnarev A G 1978 *Astron. Zh.* **55** 216
Nadezhin D K, Novikov I D and Polnarev A G 1978 *Sov. Astron.* **22** 129
[7] Novikov I D and Polnarev A G 1980 *Sov. Astron.* **24** 147
[8] Pondurets M A 1964 *Astron. Zh.* **41** 1090
Pondurets M A 1965 *Sov. Astron.* **8** 868
[9] May M M and White R H 1966 *Phys. Rev.* **141** 1232
[10] Bicknell G V and Henriksen R N 1979 *Astrophys. J.* **232** 670
[11] Novikov I D, Polnarev A G, Starobinskii A A and Zeldovich Ia B 1979 *Astron. Astrophys.* **80** 104
[12] Green A M and Liddle A R 1997 *Phys. Rev.* D **56** 6166
[13] Jedamzik K and Niemeyer J C 1999 *Phys. Rev.* D **59** 124014
[14] Khlopov M Yu and Polnarev A G 1980 *Phys. Lett.* B **97** 383
[15] Hawking S W 1989 *Phys. Lett.* B **231** 237
[16] Polnarev A G and Zembowicz R 1988 *Phys. Rev.* D **43** 1106
[17] Crawford M and Schramm D N 1982 *Nature* **298** 538

[18] Niemeyer J C and Jedamzik K 1998 *Phys. Rev. Lett.* **80** 5481
[19] Niemeyer J C and Jedamzik K 1999 *Phys. Rev.* D **59** 124013
[20] Choptuik M W 1993 *Phys. Rev. Lett.* **70** 9
[21] Gundlach C 1999 *Living Rev. Rel.* (http://www.livingreviews.org/lrr-1999-4)
[22] Shibata M and Sasaki M 1999 *Phys. Rev.* D **60** 084002
[23] Ivanov P 1998 *Phys. Rev.* D **57** 7145
[24] Green A M, Liddle A R, Malik K A and Sasaki M 2004 *Phys. Rev.* D **70** 041502
[25] Musco I, Miller J C and Rezzolla L 2005 *Class. Quantum Grav.* **22** 1405
[26] Misner C W and Sharp D H 1964 *Phys. Rev.* **136** B571
[27] Miller J C and Pantano O 1990 *Phys. Rev.* D **42** 3334
[28] Miller J C and Rezzolla L 1995 *Phys. Rev.* D **51** 4017
[29] Hernandez W C and Misner C W 1966 *Astrophys. J.* **143** 452
[30] Lifshits E M and Khalatnikov I M 1963 *Usp. Fiz. Nauk.* **80** 391
Lifshits E M and Khalatnikov I M 1964 *Sov. Phys.—Usp.* **6** 496
[31] Liddle A R and Lyth D H 2000 *Cosmological Inflation and Large-Scale Structure* (Cambridge: Cambridge University Press)
[32] Padmanabhan T 1993 *Structure Formation in the Universe* (Cambridge: Cambridge University Press)
[33] Carr B J and Hawking S W 1974 *Mon. Not. R. Astron. Soc.* **168** 399
[34] Harada T and Carr B J 2005 *Phys. Rev.* D **71** 104009
[35] Press W H, Flannery P B, Teukolsky S A and Vetterling W T 1992 *Numerical Recipes in Fortran* 2nd edn (Cambridge: Cambridge University Press)
[36] Hawke I and Stewart J M 2002 *Class. Quantum Grav.* **19** 3687
[37] Seery D and Hidalgo C 2006 *J. Cosmol. Astropart. Phys.* JCAP07(2006)008